Collision-Induced Dissociation of Homodimeric and Heterodimeric Radical Cations of 9-Methylguanine and 9-Methyl-8-oxoguanine: Correlation between Intra-Base Pair Proton Transfer Originating from the N1-H at a Watson-Crick Edge and Non-statistical Dissociation

May Myat Moe,[ab] Jonathan Benny,[ab] and Jianbo Liu*[ab]
[a] Department of Chemistry and Biochemistry, Queens College of the City University of New York, 65-30 Kissena Blvd., Queens, NY 11367, USA; [b] Ph.D. Program in Chemistry, The Graduate Center of the City University of New York, 365 5th Ave., New York, NY 10016, USA

Abstract It has been shown previously in protonated, deprotonated and ionized guanine–cytosine base pairs that intra-base pair proton transfer from the N1-H at the Watson-Crick edge of guanine to the complementary nucleobase prompts non-statistical dissociation of the base-pair system, and the dissociation of a proton-transferred base-pair structure is kinetically more favored than that of the starting, conventional base-pair structure. However, the fundamental chemistry underlying this anomalous and intriguing kinetics has not been completely revealed, which warrants the examination of more base-pair systems in different structural contexts in order to derive a generalized base-pair structure–kinetics correlation. The purpose of the present work is to expand the investigation to the non-canonical homodimeric and heterodimeric radical cations of 9-methylguaine (9MG) and 9-methyl-8-oxoguanine (9MOG), i.e., $[9MG{\cdot}9MG]^{\bullet+}$, $[9MOG{\cdot}9MG]^{\bullet+}$ and $[9MOG{\cdot}9MOG]^{\bullet+}$. Experimentally, collision-induced dissociation tandem mass spectrometry coupled with an electrospray ionization (ESI) source was used for the formation of base-pair radical cations, followed by detection of dissociation product ions and cross sections in the collisions with Xe gas under single ion-molecule collision conditions and as a function of the center-of-mass collision energy. Computationally, density functional theory and coupled cluster theory were used to calculate and identify probable base-pair structures and intra-base pair proton transfer and hydrogen transfer reactions, followed by kinetics modeling to explore the properties of dissociation transition states and kinetic factors. The significance of this work is twofold: it provides insight into base-pair opening kinetics in three biologically-important, non-canonical systems upon oxidative and ionization damage; and it links non-statistical dissociation to intra-base pair proton-transfer originating from the N1-H at the Watson-Crick edge of 8-oxoguanine, enhancing understanding towards the base-pair fragmentation assisted by proton transfer.

* E-mail: jianbo.liu@qc.cuny.edu. Tel: 1-718-997-3271.

1. Introduction

The double-helix structure of DNA is built upon hydrogen bonds (H-bonds) between complementary nucleobases. Scheme 1 indicates two types of H-bond interaction edge, taking guanosine and 8-oxoguanosine as examples.[1] The interaction through the Watson-Crick (WC)[2] edges of two complementary nucleobases usually leads to a canonical structure such as guanine–cytosine; whereas the interaction through a Hoogsteen (HG)[3-6] edge leads to a non-canonical pair formation such as guanine–guanine and its oxidized derivates. While canonical base pairs serve as the underlying principle of DNA replication and transcription; non-canonical base pairs also have great importance in DNA mutation, telomere,[7] RNA–RNA interaction and nucleoprotein complexes,[8, 9] and provide specific sites for drug, antibiotic and ion recognition.[1, 9]

We recently reported the collision-induced dissociation (CID) of the 9-methylguanine–cytosine (9MG·C) and 9-methylguanine–1-methylcytosine (9MG·1MC) base pairs in the gas phase, including protonated $[9MG + H_{N7}]^+ \cdot 1MC$ (protonated at guanine N7),[10, 11] deprotonated $9MG \cdot [C - H_{N1'}]^-$ (deprotonated at cytosine N1′-H)[12, 13] and radical cation $9MG^{\bullet+} \cdot 1MC$[14] wherein the methyl-substituents mimic the ribose sugar groups in nucleosides. A major motivation of our work was to characterize proton transfer (PT) that occur along the intra-base pair H-bonds. Intra-base pair PT not only introduces structural and energetic perturbations, but contributes to the Löwdin mechanism of spontaneous point mutations.[15-17] In addition to the biological rationale, intra-base pair PT tailors charge transfer dynamics along the DNA double helix[18] and in DNA-templated nanowires.[19] In neutral base pairs, PT in one direction is accompanied with second PT in the opposite direction to balance the charge between two nucleobases, but with a high activation barrier.[15, 17, 20-27] In protonated,[10, 11, 28-36] deprotonated,[12, 13] radical cation,[14, 20, 37-52] and radical anion base pairs[41, 53-57] and in their hydrides[33, 58] and metal cation complexes,[59-61] antiparallel double PT becomes less likely; instead, low-activation barrier single PT dominates.

Among the different ionization states of guanine–cytosine pairs we examined, $9MG \cdot [C - H_{N1'}]^-$ and $9MG^{\bullet+} \cdot 1MC$ adopt a canonical WC structure, whereas $[9MG + H_{N7}]^+ \cdot 1MC$ adopts either a WC[10] or a HG

structure[11] depending on the pH for base-pair formation. To differentiate WC vs. HG pairing, a prefix is included in the base-pair nomenclature. Capitalizing on CID tandem mass spectrometric measurements of base-pair ions, we were able to characterize intra-base pair PT dynamics. In WC-9MG$^{\bullet+}$·1MC, the N1-H (pK_a 3.9)[62] of 9MG$^{\bullet+}$ is shared with the N3′ (pKa 4.3)[63] of 1MC via an equilibrium of WC-9MG$^{\bullet+}$·1MC ⇌ WC-[9MG – H_{N1}]$^{\bullet}$·[1MC + $H_{N3'}$]$^{+}$.[14, 39, 44, 46, 49] The system is therefore composed of WC-9MG$^{\bullet+}$·1MC (referred to as a conventional conformer) and WC-[9MG – H_{N1}]$^{\bullet}$·[1MC + $H_{N3'}$]$^{+}$ (referred to as a PT conformer). The two conformers are close in energy and have nearly the same dissociation threshold energies, but they can be distinguished in CID as WC-9MG$^{\bullet+}$·1MC dissociates into 9MG$^{\bullet+}$ + 1MC whereas WC-[9MG – H_{N1}]$^{\bullet}$·[1MC + $H_{N3'}$]$^{+}$ into [9MG – H_{N1}]$^{\bullet}$ + [1MC + $H_{N3'}$]$^{+}$. An intriguing finding is that, in both Xe- and Ar-induced CID, product ions were overwhelmingly dominated by [1MC + $H_{N3'}$]$^{+}$, and product ratios are contrary to a statistical reaction model.[14] Interestingly, such non-statistical dissociation also occurs in the WC-9MG·[C – $H_{N1'}$]$^{-}$ ⇌ WC-[9MG – H_{N1}]$^{-}$·[C – $H_{N1'}$ + $H_{N3'}$] system[12] and the WC-[9MG + H_{N7}]$^{+}$·1MC ⇌ WC-[9MG + H_{N7} – H_{N1}]·[1MC + $H_{N3'}$]$^{+}$ system.[10] For each of these systems, CID is overwhelmingly dominated by the fragments generated from a PT structure, i.e., WC-[9MG – H_{N1}]$^{-}$·[C – $H_{N1'}$ + $H_{N3'}$] → [9MG – H_{N1}]$^{-}$ + [C – $H_{N1'}$ + $H_{N3'}$] and WC-[9MG + H_{N7} – H_{N1}]·[1MC + $H_{N3'}$]$^{+}$ → [9MG + H_{N7} – H_{N1}] + [1MC + $H_{N3'}$]$^{+}$.

So far only the base-pair system consisting of HG-[9MG + H_{N7}]$^{+}$·1MC ⇌ HG-9MG·[1MC + $H_{N3'}$]$^{+}$ was found to produce CID product ratios within a statistical theory framework.[11] An immediate question arising from these works is that whether non-statistical CID is a unique feature of WC-type guanine-cytosine base-pair ions. To this end, we have expanded the investigation to non-canonical base pairs consisting of the homodimeric and heterodimeric radical cations of 9MG and 9-methyl-8-oxoguanine (9MOG), i.e., [9MG·9MG]$^{\bullet+}$, [9MOG·9MG]$^{\bullet+}$ and [9MOG·9MOG]$^{\bullet+}$. Herein a superscript $^{\bullet+}$ is applied over the whole system to emphasize that base pair may undergo charge and/or spin transfer assisted by intra-base pair reactions.

[9MG·9MG]$^{\bullet+}$, [9MOG·9MG]$^{\bullet+}$ and [9MOG·9MOG]$^{\bullet+}$ were chosen to not only delineate the

correlation between base-pair structures and dissociation kinetics in different non-canonical structural contexts, but also provide significant biological implications. The guanine dimer is widely involved in telomere[7] (that plays an important role in cell division)[64] and within an RNA bulge structure (that is critical for REV protein binding to a viral site).[8] Out of the four DNA nucleobases, guanine has the lowest oxidation potential[65, 66] and with the G·G- and G·G·G-repeats the oxidation and ionization potentials become even lower.[67-70] This makes the formation of $[G\cdot G]^{\bullet+}$ and $[G\cdot G\cdot G]^{\bullet+}$ as an ultimate trap upon ionization, photooxidation and chemical oxidation of DNA and in long-range hole migration through the DNA helix.[70] The oxidation of guanine leads to a variety of biological sequelae,[71-74] of which 8-oxoguanine (OG) is the most common mutagenic lesion in genomic, mitochondrial and telomeric DNA[75] and marks oxidative stress within cells and tissues.[76, 77] The OG·G mispair may arise by the oxidatively generated damage of G·G that occurs during DNA replication.[78, 79] Because the lack of specificity in base pairing, OG also pairs with cytosine, thymine, adenine[80, 81] and with itself as well. It is worth noting that OG has an even lower oxidation potential (*i.e.*, E° vs. SHE is 0.58 V for OG[82] vs. 1.29 V for guanosine[65]), rendering the formation of $[OG\cdot G]^{\bullet+}$ and $[OG\cdot OG]^{\bullet+}$ more facile than its parent $[G\cdot G]^{\bullet+}$. Note that the lifetimes of isolated base pairs are in the range of 7 – 40 ms,[83] and base-pair opening is required in many cellular processes (e.g., sequence recognition by proteins, DNA replication and transcription).[83, 84] Particularly, the study on dissociation kinetics of $[9MG\cdot 9MG]^{\bullet+}$, $[9MOG\cdot 9MG]^{\bullet+}$ and $[9MOG\cdot 9MOG]^{\bullet+}$ will enhance the understanding of the influence of non-canonical base-pair ionization, oxidatively generated damage and tautomerization on DNA spontaneous point mutations.[15-17] To the best of our knowledge, related work on non-canonical dimeric radial cations is sparse.

2. Experimental and Theoretical Methods

2.1 Instrumentation and measurement

The experiment was carried out on our home-built guided-ion beam tandem mass spectrometer which was described elsewhere.[12, 85-87] Only critical instrumentation parameters were explicitly discussed. An electrospray ionization (ESI) source, maintained at a voltage of +2.2 kV with respect to the mass

spectrometer inlet, was used to generate a variety of $[Cu^{II}(nucleobase)_n]^{2+}$ complexes (wherein nucleobase = 9MG and/or 9MOG) from electrospray of a fresh-made mixture of 0.5 mM 9MG (Chemodex, > 98%), 0.5 mM 9MOG (provided by B. Lippert, University of Dortmund, Germany[88]) and 0.25 mM $Cu(NO_3)_2$ (Alfa Aesar, > 99.999%) in methanol/water (v : v = 3 : 1). Desolvation and transfer of the complexes to the source chamber of the mass spectrometer was made through an inlet capillary heated to 190 °C. Collisions of the complexes with the background gas within the source chamber, occurring in the region between the end of the inlet capillary (biased at +120 V with respect to ground) and a skimmer (located at the end of the source chamber and biased at +15 V with respect to ground) resulted in ejection of monomeric, homodimeric and heterodimeric radical cations of 9MG and 9MOG via redox separation reactions between Cu(II) ions and nucleobase ligands.[89-91]

Radical cations were collected into a radio-frequency (rf) hexapole ion guide, wherein ions underwent collisional damping and thermalization to 310 K.[85] Ions were subsequently transported into a quadrupole mass filter for selection of $[9MG{\cdot}9MG]^{\bullet+}$, $[9MOG{\cdot}9MG]^{\bullet+}$ or $[9MOG{\cdot}9MOG]^{\bullet+}$. Mass-selected reactant radical cations were decelerated or accelerated to a well-defined kinetic energy (E_{lab}) in the laboratory frame prior to entering a rf octopole ion guide, which was used to constrain the ions radially. Ion beam intensities were 5×10^3 counts per sec (cps) for $[9MG{\cdot}9MG]^{\bullet+}$, 5.5×10^3 cps for $[9MOG{\cdot}9MG]^{\bullet+}$ and 2×10^3 cps for $[9MOG{\cdot}9MOG]^{\bullet+}$. The full width at half maximum (FWHM) of the ion kinetic energy distribution was 0.7 eV, as measured using a retarding potential analysis technique.[92] The retarding potential analysis also allowed for the determination of the absolute zero E_{lab}.

The octopole passes through a scattering cell, in which Xe was introduced as the collision gas. The CID of base-pair radical cations was performed at a Xe pressure of 0.015 mTorr, which was sufficiently low to ensure single ion-molecule collision conditions. Fragment ions and remaining base-pair ions drifted to the end of the octopole, and were mass analyzed by a second quadrupole and counted by an electron multiplier. CID product ion cross sections were determined on the basis of reactant and product ion intensities (which were corrected for the background signal obtained when no Xe gas was introduced

to the scattering cell), the collision gas pressure and the effective cell length. Cross sections were measured as a function of collision energy (E_{col}) in the center-of-mass (CM) frame, that is $E_{col} = E_{lab} \times m_{neutral} / (m_{ion} + m_{neutral})$ where $m_{neutral}$ and m_{ion} are the masses of neutral collision gas and ions, respectively. For each E_{col}, four sets of measurements were accomplished to achieve relative uncertainties of ≤ 5%.

2.2 CID data analysis

Experimental energies available to ion-neutral collisions were broadened by the kinetic energy spread and the internal energy of reactant ions and the Doppler broadening (thermal motions) of collision gas. As a result, cross sections of CID product ions rise from zero at E_{col} before true dissociation thresholds (E_0). To extract E_0 values, CID cross sections were analyzed using a line-of-centers (LOC) model[93-96]

$$\sigma(E_{\mathrm{col}}) = \sigma_0 \frac{(E_{\mathrm{col}} + E_{\mathrm{vib}} + E_{\mathrm{rot}} - E_0)^n}{E_{\mathrm{col}}} \quad (1)$$

where σ_0 is an energy-independent scaling factor, E_{vib} and E_{rot} are reactant vibrational and rotational energies, E_0 and E_{col} are as defined above, and n is the parameter that defines the energy transfer efficiency in collisions and thus influences the slope of $\sigma(E_{col})$. This model assumes that, at the energies near E_0, at least some collisions are completely inelastic so that E_{col} is all converted to internal energy. This was verified in the threshold CID of guanine-cytosine base-pair ions and many others.[12, 14, 95]

Eqn (1) was convoluted over the experimental broadening and kinetic factors. For this purpose, a Monte Carlo simulation program[14, 97] was used to mimic experimental conditions: Xe atoms were sampling a Maxwell-Boltzmann translational kinetic energy distribution at 300 K; the base-pair radical ion beam had a kinetic energy spread of 0.7 eV, and the ion E_{vib} and E_{rot} were sampled at a temperature of 310 K. 100000 single collisions of base-pair ion with Xe were simulated at each E_{col}. The established distribution of the Xe gas velocity, and the kinetic and internal energy distributions of the base-pair ions were then sampled into $\sigma(E_{col})$ fitting. To correct for the time dependence of CID (i.e., the kinetic shift in that energy in excess of E_0 was required to produce dissociation within the experimental time scale),[98] a Rice–Ramsperger–Kassel–Marcus (RRKM, see below)[99] model was included to decide whether each collision led to detectable dissociation within the mass spectrometer ion time-of-flight (~10^2 μs). A

leveling-off collision energy was used in the fitting so that $\sigma(E_{col})$ would reach a plateau at high E_{col}. The rising curvature of $\sigma(E_{col})$ depends sensitively on E_0 and n, and their values were optimized to best reproduce the experimental data.

2.3 Reaction potential energy surface (PES) calculations

Each base-pair system includes multiple conformers due to different base-pairing motifs, keto-enol isomerization and intra-base pair PT and hydrogen transfer (HT). Conformation search was carried out using the density functional theory (DFT) ωB97XD with the 6-311++G(d,p) basis set. The ωB97XD functional[100] mitigates self-interaction errors and improves the orbital descriptions of base-pair radical cations as reported by Kumar et al.[50] The same method was used in modeling $9MG^{\bullet+}$,[86] $9MOG^{\bullet+}$,[87] and $9MG^{\bullet+}\cdot1MC$[14] reactions in our previous work, with resulting PESs consistent with experimental measurements. Basis set superposition errors (i.e., a finite basis set stabilizes the complex more than the separate components and thus overestimates binding energy[101]) for these base pairs were found to be less than 0.05 eV at the ωB97XD/6-311++G(d,p) level and therefore have no influence on the order of stability of various conformers.

Reaction coordinate was initiated at probable reacting base-pair conformations. Structures of reaction intermediates, transition states (TSs) and dissociation products were fully optimized at ωB97XD/6-311++G(d,p). TSs were verified as first-order saddle points, and the only imaginary frequencies in TSs are associated with vibration along the anticipated reaction coordinate. Intrinsic reaction coordinate calculations were carried out to ascertain that TSs are connected to correct reactant/product minima. DFT calculations were accomplished using Gaussian 16.[102]

Once reaction coordinates were identified, reaction PESs were evaluated using the domain based local pair-natural orbital coupled-cluster single-, double- and perturbative triple-excitations method DLPNO-CCSD(T)[103] coupled with the aug-cc-pVQZ basis set. This method is considered as the gold standard[104] of quantum chemistry as it provides an accuracy comparable to experiment. DLPNO-CCSD(T) calculations were accomplished using ORCA 4.2.[105] Reaction enthalpies (ΔH) reported in this

work are based on the summation of electronic energies calculated at DLPNO-CCSD(T) and 298 K thermal corrections calculated at ωB97XD, the latter included zero-point energies which were scaled by a factor 0.975.[106] The unit of eV was adopted in energy analysis so that the results may be compared directly with the ion-beam experiment.

2.4 Kinetics modeling

RRKM theory was used to predicate dissociation rate constants (k_{diss}). This theory is based on the assumption that energy is randomized and distributed statistically among all energetically accessible states in the molecule. A statistical reaction occurs via the minimum-energy pathway on reaction PES,[107] with k_{diss} proportional to the total number of energetically accessible states at the TS:[108, 109]

$$k_{\text{diss}}(E,J) = \frac{d}{h}\frac{\sum_{K=-J}^{J} G[E - E_0 - E_{\text{r}}^{\dagger}(J,K)]}{\sum_{K=-J}^{J} N[E - E_{\text{r}}(J,K)]} \quad (2)$$

where E is the system energy, E_0 is the unimolecular reaction threshold, E_r and $E_r^{\dagger}$ are the rotational energies of the reactant and the TS, d is the reaction path degeneracy, h is the Planck constant, G is the sum of states in an energy range from 0 to $E - E_0 - E_{\text{r}}^{\dagger}$ above the TS, N is the density of states in the energized reactant, J is the total angular momentum quantum number, and K is the rotation quantum number.[110] Calculation was carried out using the Zhu and Hase code of the RRKM program, [111] with N calculated using Beyer-Swinehart direct count algorithm.[112] All $(2J + 1)$ K-levels were counted.

3. Results and Discussion

3.1 Structures of [9MG·9MG]$^{\bullet+}$, [9MOG·9MG]$^{\bullet+}$ and [9MOG·9MOG]$^{\bullet+}$

Numerous tautomers were reported for neutral G·G.[1, 40, 113-129] We took the subset of tautomers in which guanine adopts the N9-H form and replaced their N9-H with a N9-methyl. The so-generated 9MG·9MG structures were subjected to geometry optimization to radical cations using ωB97XD/6-311++G(d,p). The O6-keto, O6-enol and N3-imino guanine structures as well as intra-base pair PT and HT were included in the conformation calculations. Compared to the base pairs containing an O6-keto isomer, the base pairs containing an O6-enol isomer are 0.5 eV higher in energy and those containing a N3-imino isomer are 0.64 eV higher in energy, therefore these isomers are insignificant. An attempt was

made to locate a stacking dimer,[119, 124] but such starting geometries converged to planar structures.

Therefore, we present in Scheme 2 only the ten [9MG·9MG]$^{\bullet+}$ conformers that are made of the O6-keto guanine moieties, in the order of relative energies. Their Cartesian coordinates are listed in the Supporting Information. These conformations are each featured by different H-bonds, and the pairs of PT or HT structures are indicated. The lower-energy conformations are paired through a WC-HG H-binding motif (i.e., [9MG·9MG]$^{\bullet+}$_1, 2 and 3), of which the [9MG·9MG]$^{\bullet+}$_1 conformer with the N1–H···N7′ and N2–H···O6′ bonds has an overwhelming population (99.5%). This minimum-energy structure is consistent with that reported by others.[90, 91] The radical cation in [9MG·9MG]$^{\bullet+}$_1 is located at the 9MG moiety of the WC side, which can be explained by the location of HOMO in neutral parent 9MG·9MG as shown by Figure S1 in the Supporting Information. Scheme 2 shows that a WC-WC H-binding motif reduces base-pair stability (i.e., [9MG·9MG]$^{\bullet+}$_4 and 5), and the conformations involving interaction at the ribose edge(s) have even higher energies.

The literature on 8-oxoguanine–guanine is sparse. The only reported neutral 9MOG·9MG structure consists of the N7–H···O6′ and O8···H–N1′ bonds.[79-81] On the other hand, a total of 14 conformations were identified computationally for [9MOG·9MG]$^{\bullet+}$. As shown in Scheme 3, many of these conformations are analogous to the corresponding [9MG·9MG]$^{\bullet+}$ in the context of H-bonding, i.e., pairing via N1–H···N7′ and N2–H···O6′ (WC-HG), N1–H···O6′ and N2–H···N7′ (WC-HG), N1–H···O6′ and O6···H–N1′ (WC-WC), N1–H···N3′ and O6···H–N2′, and N2–H···N3′ and N3···H–N2′, respectively, as well as their PT and HT isomers. In addition, there is a unique O8···H–N1′ bond formed only with 9MOG. Of these conformations, [9MOG·9MG]$^{\bullet+}$_1 with the WC-HG interaction dominates (population ≈ 99%). As aforementioned, 9MOG has a much lower oxidation potential than 9MG. Similarly, the adiabatic ionization energy (AIE) is 6.38 eV for 8-oxoguanine[130] and 7.75 eV for guanine.[131] As a result, radical cation is located at 9MOG in most conformations, consistent with the location of HOMO in neutral 9MOG·9MG (see Figure S2 in the Supporting Information). The exceptions are [9MOG·9MG]$^{\bullet+}$_8 and 10, for which the energies increase dramatically to compensate the differences in

nucleobase ionization energies as well as the H-bonding strength.

Finally, 11 conformations were computed for $[9MOG{\cdot}9MOG]^{\bullet+}$ as presented in Scheme 4. Each of them is paired through N1–H···O8′ and O6···H–N7′(WC-HG), N1–H···O6′ and O6···H–N1′(WC-WC), N7–H···O6′ and O6···H–N7′(HG-HG), N1–H···N3′and O6···H–N2′, N2–H···N3′ and N3···H–N2′, or its PT/HT equivalent. Similar to neutral 9MG·9MG, the HOMO in neutral 9MOG·9MOG is located at the WC side (see Figure S3 in the Supporting Information); consequently, charge and spin of $[9MOG{\cdot}9MOG]^{\bullet+}$ are centered at the WC-side.

It is possible that some rare isomers may have been missed in the conformation search, but it is less likely that we would have missed the most probable conformers in view of the good agreement with the experiment. The conformation calculations indicate that the $[9MG{\cdot}9MG]^{\bullet+}$_1 and $[9MOG{\cdot}9MG]^{\bullet+}$_1 conformers each represent the sole reactant structure for the $[9MG{\cdot}9MG]^{\bullet+}$ and $[9MOG{\cdot}9MG]^{\bullet+}$ systems and therefore were used as starting structures in PES modeling. In the following discussion, they are designated as $9MG^{\bullet+}{\cdot}9MG$ and $9MOG^{\bullet+}{\cdot}9MG$, respectively. On the other hand, the first four low-energy isomers of $[9MOG{\cdot}9MOG]^{\bullet+}$ have significant populations at room temperature, and the sum of the four accounts for a 100% population. Therefore, all of these structures are needed to take into account and deconvolute in the reactions.

3.2 CID of base-pair radical cations

3.2.1 $9MG^{\bullet+}{\cdot}9MG$ The CID data for $9MG^{\bullet+}{\cdot}9MG$ with Xe gas is summarized in Figure 1. Both $9MG^{\bullet+}$ and $[9MG + H]^+$ were detected in the mass spectrum in Figure 1a. This confirms the formation of a PT conformer $[9MG - H]^{\bullet}{\cdot}[9MG + H]^+$ in the collisional activation of the starting reactant $9MG^{\bullet+}{\cdot}9MG$. Reaction enthalpies (ΔH) for these two conformers are:

$9MG^{\bullet+}{\cdot}9MG$ (*m/z* 330)

$\rightarrow 9MG^{\bullet+}$ (*m/z* 165) + 9MG ΔH = 1.82 eV (3a)

$\rightarrow [9MG - H_{N1}]^{\bullet}{\cdot}[9MG + H_{N7'}]^+ \rightarrow [9MG + H_{N7'}]^+$ (*m/z* 166) + $[9MG - H_{N1}]^{\bullet}$ ΔH = 1.82 eV (3b)

Figures 1b and c show individual product cross sections over an E_{col} range from 0.05 to 6.0 eV. Error

bars for the cross sections were determined on the basis of the four sets of measurements. The cross section for $9MG^{\bullet+}$ rises slowly and goes through a maximum at 5 eV, while that for $[9MG + H]^+$ rises quickly and reaches a maximum at 2.4 eV. The decreasing of $[9MG + H]^+$ at high E_{col} reflects a competition between the two product channels. The cross sections were modeled for the E_{col} range up to reaching the maximum plateau using eqn (1). The values of the best fit E_0 are indicated in the figures. E_0 for reaction 3a was determined to be 1.9 ± 0.1 eV with n equal to 2.5, and E_0 for reaction 3b was determined to be 1.93 ± 0.1 eV with n equal to 1.2. The uncertainties of E_0 were determined from multiple sets of fitting by varying n and leveling off energies. The larger n value for reaction 3a explains the slower rising of the $9MG^{\bullet+}$ cross section in the near-threshold energy region.

The fact that reactions 3a and b have the nearly same E_0 but different n values implies that the two reactions have different kinetics as well as energy transfer efficiencies.[94] The correlation between the two product channels can be examined more clearly in terms of the product ratio of $[9MG + H]^+/9MG^{\bullet+}$ in Figure 1d. The plot starts from their dissociation thresholds at which both channels start to have sufficient product intensities for comparisons. The ratio of $[9MG + H]^+/9MG^{\bullet+}$ is up to 7.3 at E_{col} = 1.9 eV, decreases to 1.1 at E_{col} = 4.5 eV and drops below the unity afterwards.

In order to model base-pair kinetics, we mapped out the PES for the collisional-induced intra-base pair reactions and subsequent dissociations. Figure 2 represents the PES calculated at the DLPNO-CCSD(T)/aug-cc-pVQZ//ωB97XD/6-311++G(d,p) levels, where the starting reactant $9MG^{\bullet+}\cdot 9MG$ is located at the zero-potential energy.

As aforementioned, $9MG^{\bullet+}\cdot 9MG$ is paired via a WC-HG motif, and the radical cation is located at the WC-side. Upon collisional activation, $9MG^{\bullet+}\cdot 9MG$ undergoes PT from the N1–H at the WC-side to the N7′ at the HG-side, referred to as G_PT1 to form $[9MG - H_{N1}]^{\bullet}\cdot[9MG + H_{N7'}]^+$. Note that the activation barrier for intra-base pair PT is rather small. When comparing electronic energies only, the changes of reaction energies are $9MG^{\bullet+}\cdot 9MG \xrightarrow{TS-G\_PT1\ (\Delta E^{\neq} = 0.21\ eV)} [9MG - H_{N1}]^{\bullet}\cdot[9MG + H_{N7'}]^+$ (ΔE = 0.18 eV), with the transition state located at an energy only 0.03 eV above the product. After taking into thermal

corrections at 298 K (including ZPE), the reaction enthalpies are $9MG^{\bullet+}{\cdot}9MG \xrightarrow{TS-G\_PT1\ (\Delta H^{\neq} = 0.09\ eV)} [9MG - H_{N1}]^{\bullet}{\cdot}[9MG + H_{N7'}]^{+}$ ($\Delta H = 0.16$ eV). The reaction enthalpy of TS-G_PT1 falls below the product by 0.07 eV. This is because TS-G_PT1 has converted one vibrational mode (imaginary frequency) to the reaction coordinate and thus has less thermal correction (8.27 eV) than those of $9MG^{\bullet+}{\cdot}9MG$ (thermal correction = 8.39 eV) and $[9MG - H_{N1}]^{\bullet}{\cdot}[9MG + H_{N7'}]^{+}$ (thermal correction = 8.37 eV). In this context, PT may be assumed barrierless as depicted in Figure 2. $9MG^{\bullet+}{\cdot}9MG$ and $[9MG - H_{N1}]^{\bullet}{\cdot}[9MG + H_{N7'}]^{+}$ each dissociate to $9MG^{\bullet+} + 9MG$ and $[9MG + H_{N7'}]^{+} + [9MG - H_{N1}]^{\bullet}$, respectively, as identified in Figure 1a. The calculated dissociation threshold energies for reactions 3a and b agree with the CID data within the combined experimental and calculation uncertainties. This has verified our assignments of reacting base-pair structures. We also calculated keto-enol isomerization for $9MG^{\bullet+}{\cdot}9MG$ and $[9MG - H_{N1}]^{\bullet}{\cdot}[9MG + H_{N7'}]^{+}$. As aforementioned, the resulting isomers and their dissociation threshold energies are > 0.5 eV higher than the keto analogues, therefore are not considered further.

Assuming the relative populations of $9MG^{\bullet+}{\cdot}9MG$ and $[9MG - H_{N1}]^{\bullet}{\cdot}[9MG + H_{N7'}]^{+}$ can be represented by the ratio of their densities of state (N). The $\frac{[9MG + H_{N7'}]^{+}}{9MG^{\bullet+}}$ at each E_{col} is then given by $\frac{N_{[9MG - H_{N1}]^{\bullet}{\cdot}[9MG + H_{N7'}]^{+}}}{N_{9MG^{\bullet+}{\cdot}9MG}} \times \frac{k_{[9MG - H_{N1}]^{\bullet}{\cdot}[9MG + H_{N7'}]^{+}}}{k_{9MG^{\bullet+}{\cdot}9MG}}$ where k's are the dissociation rate constants for respective base-pair conformers. We calculated k in a statistical theory framework using eqn (2). Since there are no reverse barriers for base-pair dissociation, the dissociation process can be characterized as proceeding over TSs that are equivalent to product asymptotes. The properties of TSs may be assumed on the basis of the reactant and/or product properties. First, orbiting TSs (that are a loose association of products located at the centrifugal barriers)[98] were assumed, wherein translational modes in the TSs all converted to rotations in products. However, the dissociation time scale resulting from the calculated k's was unrealistically longer than the mass spectrometer time scale, presumably because intra-base pair interaction is stronger than typical ion-molecule association.[11, 14]

We then estimated TS properties using another two approaches.[98, 132-135] In one approach, vibrational

frequencies of the so-called ″tight″ TSs were adopted from those of base pairs, with the removal of the symmetric stretching frequency of the intra-base pair H-bonds as that corresponds to base-pair dissociation. In another approach, ″loose″ TSs were assumed for dissociation as follows. All of the base-pair frequencies that exhibit little changes in dissociation (i.e., conserved modes)[136] remain in the TSs. Of the 6 vibrational modes that are lost in two-body dissociation, the symmetric stretching of the H-bonds serves as the dissociation coordinate, and the other 5 modes (out-of-plane twisting, out-of-plane butterfly bending, anti-symmetric out-of-plane bending/step, in-plane bending/gearing and anti-symmetric stretching of the two bases) are converted to translational and rotational motions in products and their frequencies are scaled by a factor of 0.5 to reflect TS looseness and dissociation entropies. The choice of 0.5 for the scaling factor was based on the literature reports of typical non-covalently bound complexes.[11, 14, 132-134] The data resulting from the two assumptions is compared in Figure 1b, alongside the experiment. Both experiment and statistical modeling have attributed the major product ion to $[9MG + H_{N7'}]^+$. The underlying drive force is the higher proton affinity of the N7 in 9MG (965.68 kJ/mol or 10.01 eV)[137] compared to the acidity of the N1-H in $9MG^{\bullet+}$ (952 ± 10 kJ/mol or 9.87 ± 0.1 eV).[138] Other than that, neither of the two TS models is able to reproduce absolute magnitude or the E_{col}-dependence of product ratio. The statistical model predicts the increase of $[9MG + H_{N7'}]^+/9MG^{\bullet+}$ at high energies, opposite to the experiment. The contrasting difference between the experimental and the statistical theory-predicted product ratios have been observed in the CID of WC-$[9MG{\cdot}1MC]^{\bullet+}$,[14] WC-$[9MG{\cdot}1MC + H]^+$ [10] and WC-$[9MG{\cdot}C - H]^-$.[12] In all of these ″non-statistical″ systems, intra-base pair PT originating from the N1-H of guanine was involved, and the fragment ions produced by the proton-transferred base-pair structures dominated CID.

Note that Cheng *et al.*[91] inferred from their experiment that the dissociation of the guanosine dimeric radical cation $Guo^{\bullet+}{\cdot}Guo$ can be largely attributed to the formation of $[Guo + H]^+$ and $[Guo - H]^{\bullet}$. On the other hand, Feketeová *et al.*[90] reported overwhelming formation of $Guo^{\bullet+}$ but minor $[Guo + H]^+$ in the CID of $Guo^{\bullet+}{\cdot}Guo$. The contrasting product distributions in the CID of $Guo^{\bullet+}{\cdot}Guo$ by Feketeová *et al*. vs.

that of 9MG$^{\bullet+}$·9MG in the present work are not completely surprising, as the experimental conditions were different. The CID of Guo$^{\bullet+}$·Guo was carried out via low-energy, multiple collisions in which a resonance between the excitation voltage and the secular frequency of the target ion was used to induce collisions with He buffer gas in an ion trap, whereas the CID of 9MG$^{\bullet+}$·9MG was done via single collisions with Xe at well-defined E_{col} in an ion guide. Compared to single ion-gas collisions, multiple collisions facilitated energy transfer and randomization by long-time, sequential collisional activation which eventually led to statistical dissociation. In this sense, ion excitation in the ion trap was more like thermal excitation. Such contrasting CID outcomes were observed in the multiple collisions of [dGuo·deoxycytosine]$^{\bullet+}$ [52] vs. the single collisions of [9MG·1MC]$^{\bullet+}$, of which the first system presents statistical product distribution whereas the second one denotes non-statistical behavior.

3.2.2 9MOG$^{\bullet+}$·9MG Figure 3 presents the CID results of 9MOG$^{\bullet+}$·9MG, including an illustrative fragment ion mass spectrum at E_{col} = 3.0 eV, and individual product ion cross sections and product ratios as a function of E_{col}. Similar to that of 9MG$^{\bullet+}$·9MG, the CID of 9MOG$^{\bullet+}$·9MG can be described by

9MOG$^{\bullet+}$·9MG (*m/z* 346)

$\rightarrow$ 9MOG$^{\bullet+}$ (*m/z* 181) + 9MG ΔH = 1.78 eV (4a)

$\rightarrow$ [9MOG – H_{N1}]$^{\bullet}$·[9MG + $H_{N7'}$]$^{+}$ $\rightarrow$ [9MG + $H_{N7'}$]$^{+}$ (*m/z* 166) + [9MOG – H_{N1}]$^{\bullet}$ ΔH = 1.67 eV (4b)

In the PES of Figure 4, the starting reactant 9MOG$^{\bullet+}$·9MG transfers a proton from the N1-H at the WC-edge of 9MOG to the N7′ at the HG edge of 9MG (referred to as OG_PT1), yielding [9MOG – H_{N1}]$^{\bullet}$·[9MG + $H_{N7'}$]$^{+}$. Similar to the case of 9MOG$^{\bullet+}$·9MG, the transition state TS-OG_PT1 is only 0.03 eV higher in electronic energy than [9MOG – H_{N1}]$^{\bullet}$·[9MG + $H_{N7'}$]$^{+}$, and it falls below the product in the scale of reaction enthalpy when thermal corrections were taken into account. Note that aqueous pK_a was calculated to be 3.42[139] for the N1-H in 8-oxoguanine radical cation and 3.3 – 3.4 for the N7-H in [9MG + H_{N7}]$^{+}$.[140, 141] While the solution-phase pK_a cannot be directly applied to the gas phase, it agrees with the gas-phase result that reaction 4b is feasible. The two conformers were distinguished in the CID mass spectra. The LOC-fit E_0 for reaction 4a and 4b are 1.82 ± 0.1 eV (n = 2.5) and 1.72 eV ± 0.1 eV (n = 2.0),

supporting the calculated conformations.

Kinetics modeling was conducted for reactions 4a and b using the similar approaches as those for reactions 3a and b. The results are plotted in Figure 3d. Both tight- and loose-TS based RRKM predict $[9MG + H]^+$ as the dominant product ions and the ratio of $[9MG + H]^+/9MOG^{\bullet+}$ increases as decreasing E_{col}. However, neither of the two RRKM data sets reproduce the experiment quantitatively. In fact, the RRKM-predicted product ratios are a factor of 4 – 10 higher than the experiment at $E_{col} > 2$ eV and even more tremendous at low energies. It implies that the actual dissociation of $[9MOG - H]^{\bullet}\cdot[9MG + H]^+$ happened slower than a statistical predication. To this end, we did a third set of modeling by adjusting the looseness of individual dissociation TSs separately. We adopted a regular loose TS for reaction 4a by scaling the frequencies of aforementioned 5 translational and rotational modes by a factor 0.5,[11, 14, 132-134] but tightened the TS for reaction 4b by increasing the frequency scaling factor to 0.8 for the corresponding translational and rotational models so that the data could be fit to the experiment. The point was to weigh in kinetic control in additional to statistical factors. The result based on the mixed-TS modeling can be comprehended in Figure 3d, which shows a good agreement with the experiment, except at the low energies where the deviations are partially due to energy broadening in the experimental E_{col}.

3.2.3 $[9MOG\cdot9MOG]^{\bullet+}$

The CID experiment for the $[9MOG\cdot9MOG]^{\bullet+}$ system is presented in Figure 5. In contrast to the previous two systems, this system contains a total of four structures in the starting reactant ions yet only $9MOG^{\bullet+}$ was detected in the product ions at most collision energies. A trace amount of $[9MOG + H]^+$ was emerging at highest E_{col}, but the ion intensity was too low to allow for measuring its cross section.

Figure 6 includes the reactions of all four conformers of $[9MOG\cdot9MOG]^{\bullet+}$ that have contributed to reactions. These conformers are numbered (1 – 4 in gray) in the order of increasing energies calculated at ωB97XD/6-311++G(d,p), as those in Scheme 4. Note that the relative energies of conformers 1 and 4 calculated at the DLPNO-CCSD(T) level increase by 0.06 eV compared to those at the ωB97XD level, while those of conformers 2 and 3 only have minor changes at the two different levels. As a result,

relative energies and stability order of these conformers changed in the CCSD(T)-refined PES in Figure 6 compared to those in Scheme 4. But we have adopted the same set of numbering in Scheme 4 and Figure 6 to prevent confusion. To distinguish the four conformers, we indicate intra-base pair PT, HT and the interaction edge of each unit in their structural formulas. The CCSD(T)-calculated global minimum conformation is set as the zero potential energy point in the PES. Note that these conformers were made available not only in the ion source but also via intra-base pair reactions mediated by TS_OG_HT7′ and TS_OG_PT1. Note that the electronic energy of TS_OG_PT1 is higher than those of the reactant and product by only 0.05 and 0.10 eV, respectively. It drops below the reactant/product in the scale of reaction enthalpy in Figure 6b, indicating a barrierless PT for $9MOG^{\bullet+}_{WC}\cdot 9MOG_{WC}$.

As shown in the PES, the $9MOG^{\bullet+}_{WC}\cdot 9MOG_{HG}$ and $9MOG^{\bullet+}_{WC}\cdot 9MOG_{WC}$ conformers have dissociation threshold energies at 1.31 and 1.27 eV (reactions 5a and b), respectively; while the $[9MOG + H_{O6}]^{+}_{WC}\cdot[9MOG - H_{N7'}]^{\bullet}_{HG}$ and $[9MOG - H_{N1}]^{\bullet}_{WC}\cdot[9MOG + H_{O6'}]^{+}_{WC}$ conformers have dissociation thresholds at 1.94 and 1.89 eV (reactions 6a and b), respectively. As a consequence, the $9MOG^{\bullet+}_{WC}\cdot 9MOG_{HG}$ and $9MOG^{\bullet+}_{WC}\cdot 9MOG_{WC}$ structures were favored in the CID, whereas the other structures chose to interconvert *near barrierlessly* to the first two upon collisional activation rather than reach high-energy dissociation asymptotes. This seems to follow a statistical reaction model. The average E_0 value extracted from the product ion cross sections (Figure 5b) supports the calculated reaction enthalpies for reactions 5a and b. The calculation also indicates that the N1-H and N7-H in $9MOG^{\bullet+}$ have nearly the same acidity.

$$9MOG^{\bullet+}_{WC}\cdot 9MOG_{HG}\ (m/z\ 362) \rightarrow 9MOG^{\bullet+}\ (m/z\ 181) + 9MOG \qquad \Delta H = 1.31\ eV \qquad (5a)$$

$$9MOG^{\bullet+}_{WC}\cdot 9MOG_{WC}\ (m/z\ 362) \rightarrow 9MOG^{\bullet+}\ (m/z\ 181) + 9MOG \qquad \Delta H = 1.27\ eV \qquad (5b)$$

$$[9MOG + H_{O6}]^{+}_{WC}\cdot[9MOG - H_{N7'}]^{\bullet}_{HG} \rightarrow [9MOG + H_{O6}]^{+}\ (m/z\ 182) + [9MOG - H_{N7'}]^{\bullet} \qquad \Delta H = 1.94\ eV \qquad (6a)$$

$$[9MOG - H_{N1}]^{\bullet}_{WC}\cdot[9MOG + H_{O6'}]^{+}_{WC} \rightarrow [9MOG + H_{O6'}]^{+}\ (m/z\ 182) + [9MOG - H_{N1}]^{\bullet} \qquad \Delta H = 1.89\ eV \qquad (6b)$$

4. Type of canonical and non-canonical base-pair structures that induce non-statistical dissociation

It was discovered in our previous studies that singly-charged (protonated,[10] deprotonated[12] and radical cations[14]) WC-guanine–cytosine base pairs all present non-statistical dissociation kinetics. Their CID is dominated by fragment ions produced from proton-transferred base-pair conformer(s), and their product ratios deviate from statistical theory predications by at least an order of magnitude and/or follow a completely opposite energy dependence than a statistical mechanism. Those works have pinpointed intra-base pair PT from the guanine N1-H as a characteristic feature as well as a facilitator for non-statistical kinetics.

But sparingly few works have focused on the kinetics of non-canonical base pairs. To make inroads in this vein, this present work has investigated and discovered ″anomalous″ dissociation also in non-canonical base pairs. The results have provided comparisons of canonical vs. non-canonical base-pair structures and more insight into the correlation between base-pair structures and kinetics. For the $[9MG{\cdot}9MG]^{\bullet+}$ system, the reacting structures involve WC–HG interaction, and the dissociation product ratios contradict with a statistical reaction mechanism. For the $[9MOG{\cdot}9MG]^{\bullet+}$ system, the reacting structures encompass the WC-edge of 9MOG and the HG-edge of 9MG, and the dissociation product ratios also deviate from a statistical kinetics model unless when kinetic control factors were fed to the modeling. The new findings have extended the type of base-pair structure for non-statistical kinetics to include intra-base pair PT from the N1-H in 8-oxoguanine, and reaffirmed the importance of H-bonds at the WC-side.

We are currently investigating another two systems, $[9MOG{\cdot}1MC]^{\bullet+}$ and [9MOG·9-methyladenine]$^{\bullet+}$, each of which involves the WC and HG side of 9MOG, respectively. The ultimate purpose is to extract a more general description of key structures that are needed for non-statistical kinetics. The combination of these results will be used to design a model system for conducting molecular dynamics simulation, from which the fundamental chemistry underlying the intriguing base-pair reactions may be disentangled and fully revealed.

4. Conclusions

Dissociation of three non-canonical base-pair systems made up of the radical cation of the homo- and hetero-dimers of 9MG and 9MOG were measured using CID tandem mass spectrometry and calculated using density functional theory and coupled cluster theory. All the reacting base pairs involve intra-base pair PT originating from the N1-H of 9MG or 9MOG. Base-pair dissociation, interrogated by the measurements of product ion cross sections and product ratios, have demonstrated non-statistical dissociation kinetics for $[9MG{\cdot}9MG]^{\bullet+}$ and $[9MOG{\cdot}9MG]^{\bullet+}$. The dissociation of a proton-transferred conformer is more favored than that of the parent, conventional conformer, i.e., $[9MG - H_{N1}]^{\bullet}{\cdot}[9MG + H_{N7'}]^{+} \rightarrow [9MG - H_{N1}]^{\bullet} + [9MG + H_{N7'}]^{+} >> 9MG^{\bullet+}{\cdot}9MG \rightarrow 9MG^{\bullet+} + 9MG$, and $[9MOG - H_{N1}]^{\bullet}{\cdot}[9MG + H_{N7'}]^{+} \rightarrow [9MOG - H_{N1}]^{\bullet} + [9MG + H_{N7'}]^{+} >> 9MOG^{\bullet+}{\cdot}9MG \rightarrow 9MOG^{\bullet+} + 9MG$, despite the pair of two dissociation channels for each system has the nearly same dissociation threshold. The $[9MOG{\cdot}9MOG]^{\bullet+}$ system appears to follow the minimum-energy reaction pathway which leads to dissociation occurring only in $9MOG^{\bullet+}{\cdot}9MOG$ but not its PT or HT isomers. This is because the dissociation energies leading to $9MOG^{\bullet+} + 9MOG$ is 0.6 eV lower than those leading to $[9MOG + H]^{+} + [9MOG - H]^{\bullet}$. As a consequence, thermodynamics becomes the dominating factor in determining dissociation outcomes and overrides any non-statistical kinetics that may exist. The present work has not only supported our previous observations that non-statistical reaction is correlated to intra-base pair proton transfer at the WC-edge of guanine but extended this finding to the 8-oxoguanine nucleobase and to non-canonical base pairs. The impact of this work goes beyond base-pair kinetics. It adds to the work focusing on ionization and oxidatively generated damage in non-canonical guanine base pairs and the influence of resulting base-pair tautomerization and opening on DNA spontaneous point mutations, and is related to the design of DNA-templated nanodevices.

Supporting Information

HOMOs in 9MG·9MG, 9MOG·9MG and 9MOG·9MOG. Cartesian coordinates for calculated structures.

Acknowledgements

This work was supported by National Science Foundation (Grant No. CHE 1856362). We are grateful to

Professor Bernhard Lippert (University of Dortmund, Germany) for providing us 9MOG.

References

1 S. T. Madariaga and J. G. Contreras, *J. Chil. Chem. Soc.*, 2010, **55**, 50-52.
2 J. D. Watson and F. H. C. Crick, *Nature*, 1953, **171**, 737-738.
3 K. Hoogsteen, *Acta Crystallogr.*, 1959, **12**, 822-823.
4 K. Hoogsteen, *Acta Crystallographica*, 1963, **16**, 907-916.
5 Y. Courtois, P. Fromageot and W. Guschlbauer, *Eur. J. Biochem.*, 1968, **6**, 493-501.
6 G. J. Quigley, G. Ughetto, G. A. Van der Marel, J. H. Van Boom, A. H. J. Wang and A. Rich, *Science*, 1986, **232**, 1255-1258.
7 E. Henderson, C. C. Hardin, S. K. Walk, I. Tinoco, Jr. and E. H. Blackburn, *Cell*, 1987, **51**, 899-908.
8 D. P. Bartel, M. L. Zapp, M. R. Green and J. W. Szostak, *Cell*, 1991, **67**, 529-536.
9 T. Hermann and E. Westhof, *Chem. Biol.*, 1999, **6**, R335-R343.
10 Y. Sun, M. M. Moe and J. Liu, *Phys. Chem. Chem. Phys.*, 2020, **22**, 24986-25000.
11 M. m. Moe, J. Benny, Y. Sun and J. Liu, *Phys. Chem. Chem. Phys.*, 2021, **23**, 9365-9380.
12 W. Lu and J. Liu, *Phys. Chem. Chem. Phys.*, 2016, **18**, 32222-32237.
13 J. Liu, *Phys. Chem. Chem. Phys.*, 2017, **19**, 30616-30626.
14 Y. Sun, M. M. Moe and J. Liu, *Phys. Chem. Chem. Phys.*, 2020, **20**, 14875-14888.
15 P. O. Löwdin, *Rev. Mod. Phys.*, 1963, **35**, 724-732, discussion 732-723.
16 L.-Y. Fu, G.-Z. Wang, B.-G. Ma and H.-Y. Zhang, *Biochem. Biophys. Res. Commun.*, 2011, **409**, 367-371.
17 A. Gheorghiu, P. V. Coveney, A. A. Arabi, P. V. Coveney and A. A. Arabi, *Interface Focus*, 2020, **10**, 20190120.
18 K. Kawai, Y. Osakada and T. Majima, *ChemPhysChem*, 2009, **10**, 1766-1769.
19 Q. Gu and D. T. Haynie, *Annu. Rev. Nano Res.*, 2008, **2**, 217-285.
20 J. Bertran, A. Oliva, L. Rodriguez-Santiago and M. Sodupe, *J. Am. Chem. Soc.*, 1998, **120**, 8159-8167.
21 L. Gorb, Y. Podolyan, P. Dziekonski, W. A. Sokalski and J. Leszczynski, *J. Am. Chem. Soc.*, 2004, **126**, 10119-10129.
22 Y. Lin, H. Wang, S. Gao, R. Li and H. F. Schaefer, III, *J. Phys. Chem. B*, 2012, **116**, 8908-8915.
23 V. Sauri, J. P. Gobbo, J. J. Serrano-Pérez, M. Lundberg, P. B. Coto, L. Serrano-Andrés, A. C. Borin, R. Lindh, M. Merchán and D. Roca-Sanjuán, *J. Chem. Theory Comput.*, 2013, **9**, 481-496.
24 R. R. Q. Freitas, R. Rivelino, F. d. B. Mota, G. K. Gueorguiev and C. M. C. de Castilho, *J. Phys. Chem. C*, 2015, **119**, 15735-15741.
25 Y. Zhang, M. Sun and Y. Li, *Sci. Rep.*, 2016, **6**, 25568.
26 E. E. Romero and F. E. Hernandez, *Phys. Chem. Chem. Phys.*, 2018, **20**, 1198-1209.
27 A. A. Arabi and C. F. Matta, *J. Phys. Chem. B*, 2018, **122**, 8631-8641.
28 G. P. Ford and B. Wang, *Int. J. Quantum Chem.*, 1992, **44**, 587-603.
29 M. Noguera, M. Sodupe and J. Bertrán, *Theor. Chem. Acc.*, 2004, **112**, 318-326.
30 S. Y. Han, S. H. Lee, J. Chung and H. B. Oh, *J. Chem. Phys.*, 2007, **127**, 245102.
31 Y. Lin, H. Wang, S. Gao and H. F. Schaefer, III, *J. Phys. Chem. B*, 2011, **115**, 11746–11756.
32 Y. Seong, S. Y. Han, S.-C. Jo and H. B. Oh, *Mass Spectrom. Lett.*, 2011, **2**, 73-75.
33 Y. Lin, H. Wang, Y. Wu, S. Gao and H. F. Schaefer, III, *Phys. Chem. Chem. Phys.*, 2014, **16**, 6717-6725.
34 A. F. Cruz-Ortiz, M. Rossa, F. Berthias, M. Berdakin, P. Maitre and G. A. Pino, *J. Phys. Chem. Lett.*, 2017, **8**, 5501-5506.
35 J. Jun and S. Y. Han, *Theor. Chem. Acc.*, 2017, **136**, 1-10.
36 J. J. Park, C. S. Lee and S. Y. Han, *J. Am. Soc. Mass Spectrom.*, 2018, **29**, 2368-2379.
37 K. Hildenbrand and D. Schulte-Frohlinde, *Free Radical Res. Commun.*, 1990, **11**, 195-206.
38 A. O. Colson, B. Besler and M. D. Sevilla, *J. Phys. Chem.*, 1992, **96**, 9787-9794.
39 M. Hutter and T. Clark, *J. Am. Chem. Soc.*, 1996, **118**, 7574-7577.
40 E. Nir, K. Kleinermanns and M. S. de Vries, *Nature*, 2000, **408**, 949-950.
41 X. Li, Z. Cai and M. D. Sevilla, *J. Phys. Chem. B*, 2001, **105**, 10115-10123.
42 K. Kobayashi and S. Tagawa, *J. Am. Chem. Soc.*, 2003, **125**, 10213-10218.
43 A. K. Ghosh and G. B. Schuster, *J. Am. Chem. Soc.*, 2006, **128**, 4172-4173.
44 K. Kobayashi, R. Yamagami and S. Tagawa, *J. Phys. Chem. B*, 2008, **112**, 10752-10757.

45 A. Kumar and M. D. Sevilla, *J. Phys. Chem. B*, 2009, **113**, 11359-11361.
46 A. W. Parker, C. Y. Lin, M. W. George, M. Towrie and M. K. Kuimova, *J. Phys. Chem. B*, 2010, **114**, 3660-3667.
47 J. P. Ceron-Carrasco, A. Requena, E. A. Perpete, C. Michaux and D. Jacquemin, *J. Phys. Chem. B*, 2010, **114**, 13439-13445.
48 S. Steenken and J. Reynisson, *Phys. Chem. Chem. Phys.*, 2010, **12**, 9088-9093.
49 Y. Rokhlenko, J. Cadet, N. E. Geacintov and V. Shafirovich, *J. Am. Chem. Soc.*, 2014, **136**, 5956-5962.
50 A. Kumar and M. D. Sevilla, *J. Phys. Chem. B*, 2014, **118**, 5453-5458.
51 J. Jie, K. Liu, L. Wu, H. Zhao, D. Song and H. Su, *Sci. Adv.*, 2017, **3**, e1700171.
52 L. Feketeová, B. Chan, G. N. Khairallah, V. Steinmetz, P. Maitre, L. Radom and R. A. J. O'Hair, *J. Phys. Chem. Lett.*, 2017, **8**, 3159-3165.
53 H.-Y. Chen, C.-L. Kao and S. C. N. Hsu, *J. Am. Chem. Soc.*, 2009, **131**, 15930-15938.
54 A. Szyperska, J. Rak, J. Leszczynski, X. Li, Y. J. Ko, H. Wang and K. H. Bowen, *ChemPhysChem*, 2010, **11**, 880-888.
55 H.-Y. Chen, S.-W. Yeh, S. C. N. Hsu, C.-L. Kao and T.-Y. Dong, *Phys. Chem. Chem. Phys.*, 2011, **13**, 2674-2681.
56 A. Gupta, H. M. Jaeger, K. R. Compaan and H. F. Schaefer, III, *J. Phys. Chem. B*, 2012, **116**, 5579-5587.
57 J. Gu, J. Wang and J. Leszczynski, *J. Phys. Chem. B*, 2015, **119**, 2454-2458.
58 J. D. Zhang, Z. Chen and H. F. Schaefer, III, *J. Phys. Chem. A*, 2008, **112**, 6217-6226.
59 J. Bertran, M. Noguera and M. Sodupe, in *Fundamental World of Quantum Chemistry*, ed. E. J. Braendas and E. S. Kryachko, Kluwer Academic Publishers, 2003, vol. 2, pp. 557-581.
60 Y. Han and D. Li, *J. Mol. Model*, 2019, **25**, 40.
61 A. F. Cruz-Ortiz, R. A. Jara-Toro, M. Berdakin, E. Loire and G. A. Pino, *Eur. Phys. J. D*, 2021, **75**, 119.
62 L. P. Candeias and S. Steenken, *J. Am. Chem. Soc.*, 1989, **111**, 1094-1099.
63 J. A. Dean, *Lange's Handbook of Chemistry, Fifteenth Edition*, McGraw-Hill, New York, 1999.
64 C. B. Harley, A. B. Futcher and C. W. Greider, *Nature*, 1990, **345**, 458-460.
65 S. Steenken and S. V. Jovanovic, *J. Am. Chem. Soc.*, 1997, **119**, 617-618.
66 K. Lewis, K. Copeland and G. Hill, *Int. J. Quantum Chem.*, 2014, **114**, 1678-1684.
67 J. Reynisson and S. Steenken, *Phys. Chem. Chem. Phys.*, 2002, **4**, 5346-5352.
68 I. Saito, M. Takayama, H. Sugiyama, K. Nakatani, A. Tsuchida and M. Yamamoto, *J. Am. Chem. Soc.*, 1995, **117**, 6406-6407.
69 H. Sugiyama and I. Saito, *J. Am. Chem. Soc.*, 1996, **118**, 7063-7068.
70 I. Saito, T. Nakamura, K. Nakatani, Y. Yoshioka, K. Yamaguchi and H. Sugiyama, *J. Am. Chem. Soc.*, 1998, **120**, 12686-12687.
71 J. Cadet, M. Berger, G. W. Buchko, P. C. Joshi, S. Raoul and J.-L. Ravanat, *J. Am. Chem. Soc.*, 1994, **116**, 7403-7404.
72 J. Cadet, T. Douki and J.-L. Ravanat, *Acc. Chem. Res.*, 2008, **41**, 1075-1083.
73 W. L. Neeley and J. M. Essigmann, *Chem. Res. Toxicol.*, 2006, **19**, 491-505.
74 A. M. Fleming and C. J. Burrows, *Free Radic. Biol. Med.*, 2017, **107**, 35-52.
75 J. Cadet and P. D. Mascio, in *Modified nucleosides: In Biochemistry, Biotechnology and Medicine*, ed. P. Herdewijn, Wiley-VCH Verlag Gmbh & Co. KGaA, Weinheim, 2008, pp. 29-47.
76 S. Boiteux and J. P. Radicella, *Biochimie*, 1999, **81**, 59-67.
77 H. Sies, *Oxidative Stress*, Academic Press, 1985.
78 V. Thiviyanathan, A. Somasunderam, T. K. Hazra, S. Mitra and D. G. Gorenstein, *J. Mol. Biol.*, 2003, **325**, 433-442.
79 J. Šponer, P. Jurečka and P. Hobza, *J. Am. Chem. Soc.*, 2004, **126**, 10142-10151.
80 J. Reynisson and S. Steenken, *J. Mol. Struct.: Theochem*, 2005, **723**, 29-36.
81 H. Fujimoto, M. Pinak, T. Nemoto and J. K. Bunta, *Cent. Eur. J. Phys.*, 2007, **5**, 49-61.
82 H. Yanagawa, Y. Ogawa and M. Ueno, *J. Biol. Chem.*, 1992, **267**, 13320-13326.
83 U. Dornberger, M. Leijon and H. Fritzsche, *J. Biol. Chem.*, 1999, **274**, 6957-6962.
84 A. M. Ababneh, C. C. Large and S. Georghiou, *Biophys. J.*, 2003, **85**, 1111-1127.
85 Y. Fang and J. Liu, *J. Phys. Chem. A*, 2009, **113**, 11250-11261.
86 Y. Sun, M. Tsai, M. M. Moe and J. Liu, *J. Phys. Chem. A*, 2021, **125**, 1564-1576.

87 M. M. Moe, M. Tsai and J. Liu, *ChemPlusChem*, 2021, **86**, 1243-1254.
88 R. K. O. Sigel, E. Freisinger and B. Lippert, *JBIC, J. Biol. Inorg. Chem.*, 2000, **5**, 287-299.
89 I. K. Chu, C. F. Rodriquez, T.-C. Lau, A. C. Hopkinson and K. W. M. Siu, *J. Phys. Chem. B*, 2000, **104**, 3393-3397.
90 L. Feketeová, E. Yuriev, J. D. Orbell, G. N. Khairallah and R. A. J. O'Hair, *Int. J. Mass Spectrom.*, 2011, **304**, 74-82.
91 P. Cheng and D. K. Bohme, *J. Phys. Chem. B*, 2007, **111**, 11075-11082.
92 K. M. Ervin and P. B. Armentrout, *J. Chem. Phys.*, 1985, **83**, 166-189.
93 C. Rebick and R. D. Levine, *J. Chem. Phys.*, 1973, **58**, 3942-3952.
94 R. D. Levine and R. B. Bernstein, *Molecular Reaction Dynamics and Chemical Reactivity*, Oxford University Press, New York, 1987.
95 P. B. Armentrout, *Int. J. Mass Spectrom.*, 2000, **200**, 219-241.
96 J. Liu, B. van Devener and S. L. Anderson, *J. Chem. Phys.*, 2002, **116**, 5530-5543.
97 M. B. Sowa-Resat, P. A. Hintz and S. L. Anderson, *J. Phys. Chem.*, 1995, **99**, 10736-10741.
98 M. T. Rodgers, K. M. Ervin and P. B. Armentrout, *J. Chem. Phys.*, 1997, **106**, 4499-4508.
99 R. A. Marcus, *J. Chem. Phys.*, 1952, **20**, 359-364.
100 J.-D. Chai and M. Head-Gordon, *Phys. Chem. Chem. Phys.*, 2008, **10**, 6615-6620.
101 F. B. van Duijneveldt, J. G. C. M. van Duijneveldt-van de Rijdt and J. H. van Lenthe, *Chem. Rev.*, 1994, **94**, 1873-1885.
102 M. J. Frisch, G. W. Trucks, H. B. Schlegel, G. E. Scuseria, M. A. Robb, J. R. Cheeseman, G. Scalmani, V. Barone, G. A. Petersson, H. Nakatsuji, X. Li, M. Caricato, A. V. Marenich, J. Bloino, B. G. Janesko, R. Gomperts, B. Mennucci, H. P. Hratchian, J. V. Ortiz, A. F. Izmaylov, J. L. Sonnenberg, Williams, F. Ding, F. Lipparini, F. Egidi, J. Goings, B. Peng, A. Petrone, T. Henderson, D. Ranasinghe, V. G. Zakrzewski, J. Gao, N. Rega, G. Zheng, W. Liang, M. Hada, M. Ehara, K. Toyota, R. Fukuda, J. Hasegawa, M. Ishida, T. Nakajima, Y. Honda, O. Kitao, H. Nakai, T. Vreven, K. Throssell, J. A. Montgomery Jr., J. E. Peralta, F. Ogliaro, M. J. Bearpark, J. J. Heyd, E. N. Brothers, K. N. Kudin, V. N. Staroverov, T. A. Keith, R. Kobayashi, J. Normand, K. Raghavachari, A. P. Rendell, J. C. Burant, S. S. Iyengar, J. Tomasi, M. Cossi, J. M. Millam, M. Klene, C. Adamo, R. Cammi, J. W. Ochterski, R. L. Martin, K. Morokuma, O. Farkas, J. B. Foresman and D. J. Fox, Gaussian 16 Rev. B.01, Wallingford, CT, 2016.
103 D. G. Liakos, M. Sparta, M. K. Kesharwani, J. M. L. Martin and F. Neese, *J. Chem. Theory Comput.*, 2015, **11**, 1525-1539.
104 K. Raghavachari, G. W. Trucks, J. A. Pople and M. Head-Gordon, *Chem. Phys. Lett.*, 1989, **157**, 479-483.
105 F. Neese, *WIREs Comput Mol Sci*, 2018, **8**, e1327.
106 I. M. Alecu, J. Zheng, Y. Zhao and D. G. Truhlar, *J. Chem. Theory Comput.*, 2010, **6**, 2872-2887.
107 K. Fukui, *J. Phys. Chem.*, 1970, **74**, 461-463.
108 T. Baer and W. L. Hase, *Unimolecular reaction dynamics: Theory and experiments*, Oxford University Press, New York, 1996.
109 W. L. Hase, *Acc. Chem. Res.*, 1998, **31**, 659-665.
110 L. Zhu and W. L. Hase, *Chem. Phys. Lett.*, 1990, **175**, 117-124.
111 L. Zhu and W. L. Hase, A General RRKM Program (QCPE 644), Quantum Chemistry Program Exchange, Chemistry Department, University of Indiana, Bloomington, 1993.
112 T. Beyer and D. F. Swinehart, *Commun. ACM*, 1973, **16**, 379.
113 P. Hobza and C. Sandorfy, *J. Am. Chem. Soc.*, 1987, **109**, 1302-1307.
114 J. Šponer, J. Leszczynski and P. Hobza, *J. Phys. Chem.*, 1996, **100**, 1965-1974.
115 P. Hobza and J. Sponer, *Chem. Phys. Lett.*, 1996, **261**, 379-384.
116 J. Florián, J. Šponer and A. Warshel, *J. Phys. Chem. B*, 1999, **103**, 884-892.
117 P. Hobza and J. Sponer, *Chem. Rev.*, 1999, **99**, 3247-3276.
118 E. Nir, C. Janzen, P. Imhof, K. Kleinermanns and M. S. de Vries, *Phys. Chem. Chem. Phys.*, 2002, **4**, 740-750.
119 P. Hobza and J. Sponer, *J. Am. Chem. Soc.*, 2002, **124**, 11802-11808.
120 E. Nir, C. Pluetzer, K. Kleinermanns and M. de Vries, *Eur. Phys. J. D*, 2002, **20**, 317-329.
121 P. Hobza and V. Spirko, *Phys. Chem. Chem. Phys.*, 2003, **5**, 1290-1294.
122 J. Sponer and P. Hobza, *Collect. Czech. Chem. Commun.*, 2003, **68**, 2231-2282.

123 A. Abo-Riziq, B. Crews, L. Grace and M. S. de Vries, *J. Am. Chem. Soc.*, 2005, **127**, 2374-2375.
124 S.-h. Urashima, H. Asami, M. Ohba and H. Saigusa, *J. Phys. Chem. A*, 2010, **114**, 11231-11237.
125 A. K. Jissy and A. Datta, *ChemPhysChem*, 2012, **13**, 4163-4172.
126 J. Zhao, M. Wang, H. Yang, M. Zhang, P. Liu and Y. Bu, *J. Phys. Chem. B*, 2013, **117**, 10698-10710.
127 A. Halder, S. Bhattacharya, A. Datta, D. Bhattacharyya and A. Mitra, *Phys. Chem. Chem. Phys.*, 2015, **17**, 26249-26263.
128 A. Ungordu and N. Tezer, *J. Mol. Graphics Modell.*, 2017, **74**, 265-272.
129 N. J. Thornton and T. van Mourik, *Int. J. Mol. Sci.*, 2020, **21**, 6571.
130 F. Prat, K. N. Houk and C. S. Foote, *J. Am. Chem. Soc.*, 1998, **120**, 845-846.
131 J. Zhou, O. Kostko, C. Nicolas, X. Tang, L. Belau, M. S. de Vries and M. Ahmed, *J. Phys. Chem. A*, 2009, **113**, 4829-4832.
132 F. Meyer, F. A. Khan and P. B. Armentrout, *J. Am. Chem. Soc.*, 1995, **117**, 9740-9748.
133 M. B. More, E. D. Glendening, D. Ray, D. Feller and P. B. Armentrout, *J. Phys. Chem.*, 1996, **100**, 1605-1614.
134 D. Ray, D. Feller, M. B. More, E. D. Glendening and P. B. Armentrout, *J. Phys. Chem.*, 1996, **100**, 16116-16125.
135 M. T. Rodgers and P. B. Armentrout, *J. Chem. Phys.*, 1998, **109**, 1787-1800.
136 S. J. Klippenstein, A. L. L. East and W. D. Allen, *J. Chem. Phys.*, 1994, **101**, 9198-9201.
137 J. J. Park and S. Y. Han, *J. Am. Soc. Mass Spectrom.*, 2019, **30**, 846-854.
138 L. Feketeová, G. N. Khairallah, B. Chan, V. Steinmetz, P. Maître, L. Radom and R. A. J. O'Hair, *Chem. Commun.* , 2013, **49**, 7343-7345.
139 S. Wei, Z. Zhang, S. Liu and Y. Wang, *New J. Chem.*, 2021, **45**, 11202-11212.
140 V. Verdolino, R. Cammi, B. H. Munk and H. B. Schlegel, *J. Phys. Chem. B*, 2008, **112**, 16860-16873.
141 B. Thapa and H. B. Schlegel, *J. Phys. Chem. A*, 2015, **119**, 5134-5144.

Scheme 1. Different edges in guanosine and 8-oxoguanosine, including atomic numbering.

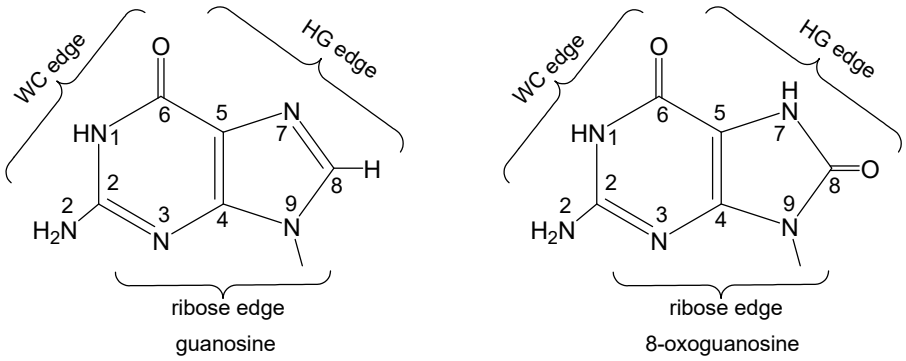

Scheme 2. Relative enthalpies of various [9MG·9MG]$^{\bullet+}$ conformers calculated at ωB97XD/ 6-311++G(d,p), including thermal corrections at 298 K. Cartesian coordinates of these conformers are reported in the Supporting Information. PT1, PT2 and HT1 represent atom position-specific proton and hydrogen transfer from the left 9MG to the right, while PT2′ represents a transfer in an opposite direction.

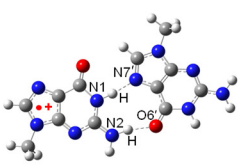

[9MG·9MG]$^{\bullet+}$_1
ΔH = 0.0 eV
Population = 99.5%

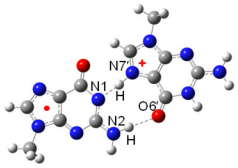

2 ($\xleftarrow{PT1}$ 1)
0.14 eV
0.4%

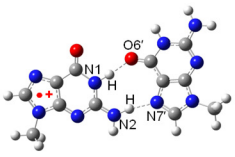

3
0.17 eV
0.1%

4
0.38 eV
< 0.1 %

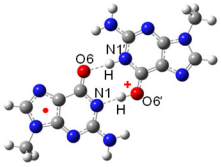

5 ($\xleftarrow{PT1}$ 4)
0.40 eV

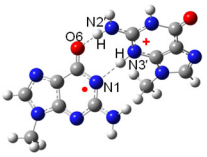

6 ($\xleftarrow{HT1}$ 7)
0.94 eV

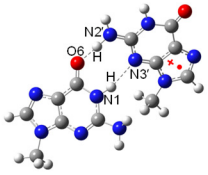

7
0.95 eV

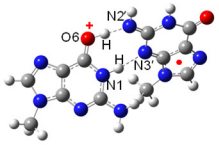

8 ($\xleftarrow{PT2'}$ 7)
1.03 eV

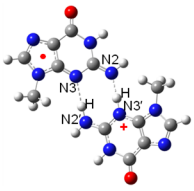

9 ($\xleftarrow{PT2}$ 10)
1.31 eV

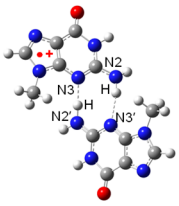

10
1.40 eV

Scheme 3. Relative enthalpies of various $[9MOG{\cdot}9MG]^{\bullet+}$ conformers calculated at ωB97XD/ 6-311++G(d,p) , including thermal corrections at 298 K. Cartesian coordinates of these conformers are reported in the Supporting Information. PT1, PT2, HT1 and HT7 represent atom position-specific proton and hydrogen transfer from 9MOG to 9MG, while PT2′, HT1′ and HT2′ represent transfer in an opposite direction.

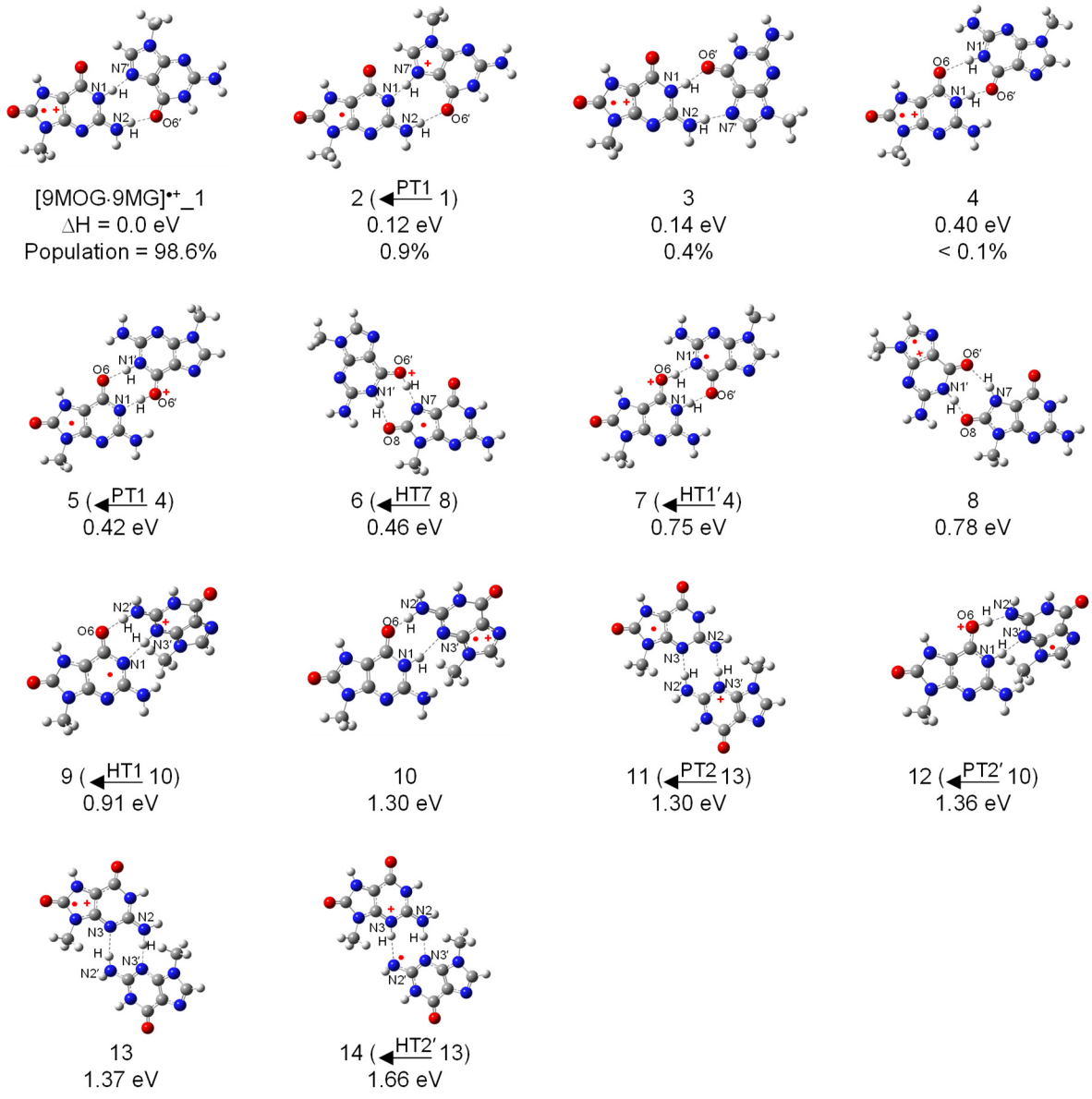

Scheme 4. Relative enthalpies of various [9MOG·9MOG]$^{\bullet+}$ conformers calculated at ωB97XD/ 6-311++G(d,p), including thermal corrections at 298 K. Cartesian coordinates of these conformers are reported in the Supporting Information. PT1, PT2, PT7 and HT1 represent atom position-specific proton and hydrogen transfer from the left 9MOG to the right, while PT2′ and HT7′ represent transfer in an opposite direction.

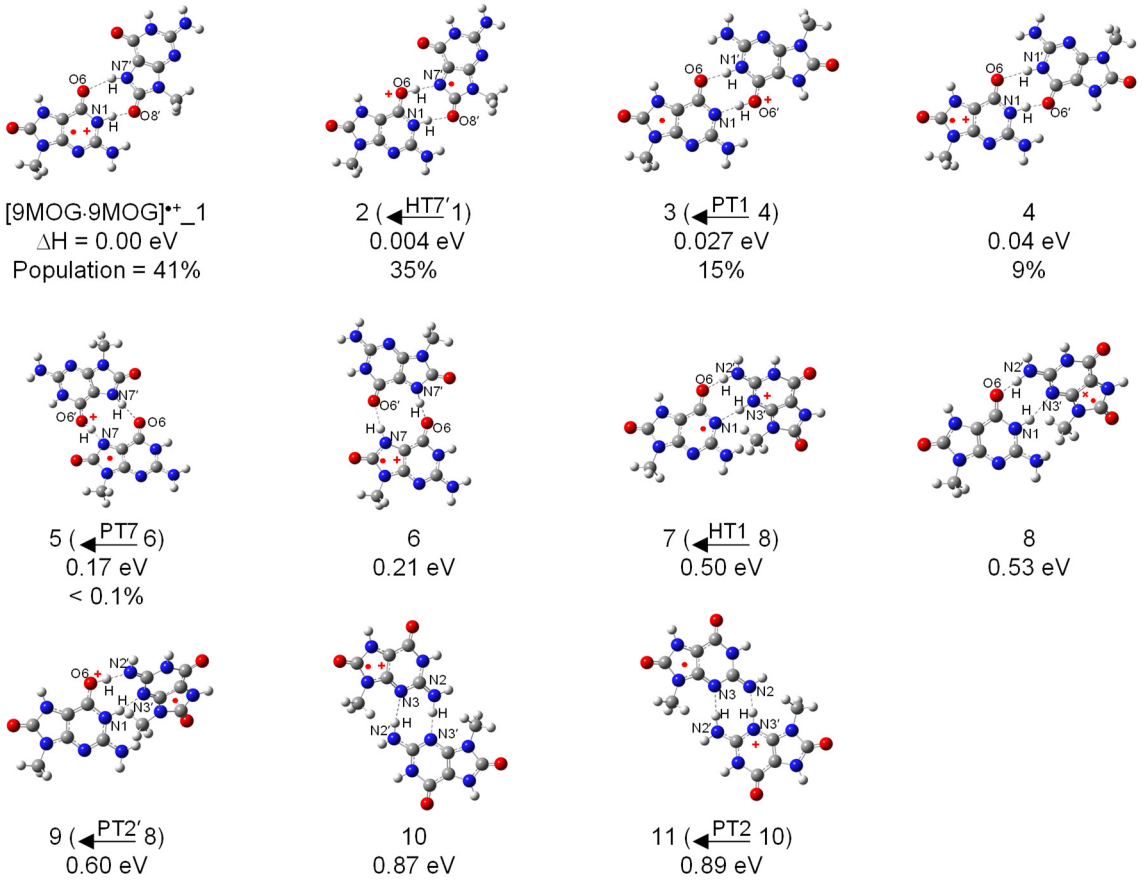

Figure Caption

Fig. 1 (a) CID product ion mass spectrum of $[9MG \cdot 9MG]^{\bullet+}$ with Xe at E_{col} = 4.0 eV; (b, c) individual product ion cross sections, and (d) product ratio of $[9MG + H]^{+}/9MG^{\bullet+}$ as discussed in the text.

Fig. 2 PES for intra-base pair PT and dissociation of $9MG^{\bullet+} \cdot 9MG$. Reaction enthalpies were calculated at DLPNO-CCSD(T)/aug-cc-PVQZ//ωB97XD/6-311++G(d,p), including thermal corrections at 298 K.

Fig. 3 (a) CID product ion mass spectrum of $[9MOG \cdot 9MG]^{\bullet+}$ with Xe at E_{col} = 3.0 eV; (b, c) individual product ion cross sections, and (d) product ratio of $[9MG + H]^{+}/9MOG^{\bullet+}$ as discussed in the text.

Fig. 4 PES for intra-base pair PT and dissociation of $9MOG^{\bullet+} \cdot 9MG$. Reaction enthalpies were calculated at DLPNO-CCSD(T)/aug-cc-PVQZ//ωB97XD/6-311++G(d,p), including thermal corrections at 298 K.

Fig. 5 (a) CID product ion mass spectrum of $[9MOG \cdot 9MOG]^{\bullet+}$ with Xe at E_{col} = 5.0 eV; and (b) product ion cross sections.

Fig. 6 PES for intra-base pair PT, HT and dissociation of $[9MOG \cdot 9MOG]^{\bullet+}$. Reaction enthalpies were calculated at DLPNO-CCSD(T)/aug-cc-PVQZ//ωB97XD/6-311++G(d,p), including thermal corrections at 298 K.

Fig. 1

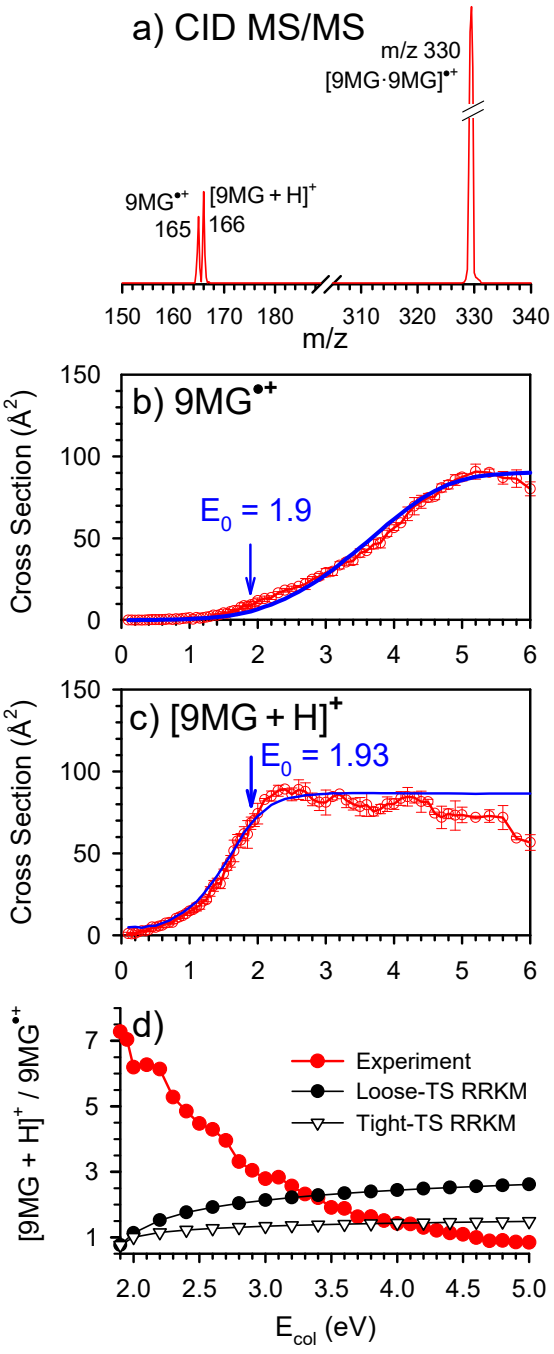
a) CID MS/MS
m/z 330
[9MG·9MG]•+
9MG•+
165
[9MG + H]+
166
150 160 170 180 310 320 330 340
m/z
b) 9MG•+
E0 = 1.9
Cross Section (Å2)
c) [9MG + H]+
E0 = 1.93
Cross Section (Å2)
d)
Experiment
Loose-TS RRKM
Tight-TS RRKM
[9MG + H]+ / 9MG•+
Ecol (eV)

Fig. 2

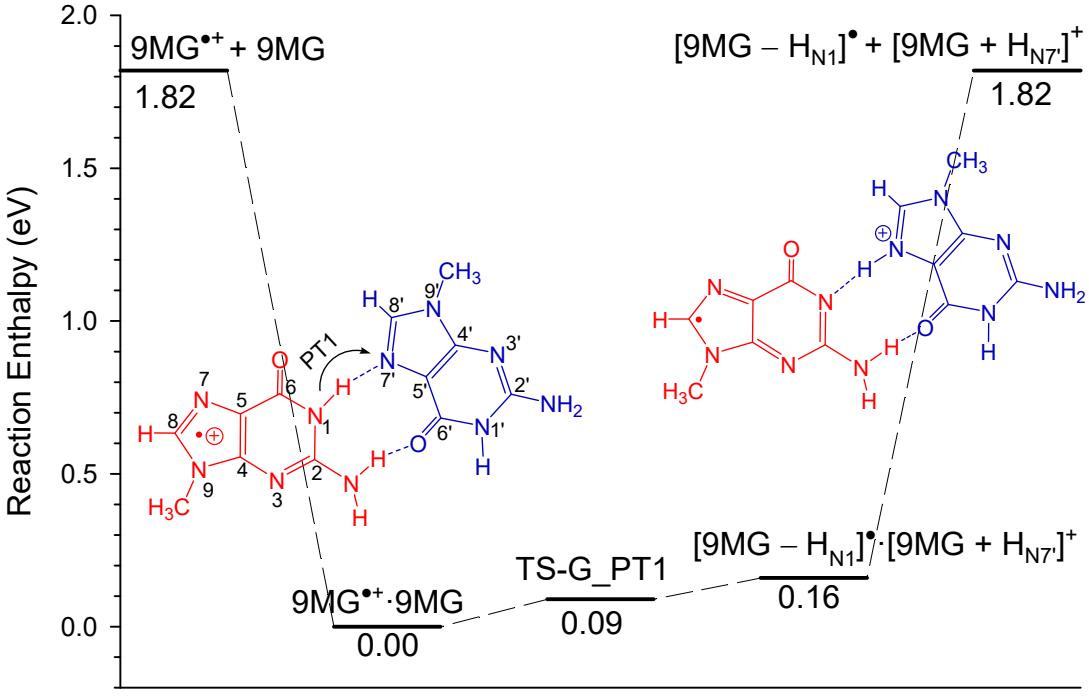
Reaction Enthalpy (eV)
2.0
1.5
1.0
0.5
0.0
9MG•+ + 9MG
1.82
9MG•+·9MG
0.00
TS-G_PT1
0.09
[9MG – HN1]• + [9MG + HN7']+
1.82
[9MG – HN1]•·[9MG + HN7']+
0.16
PT1

Fig. 3

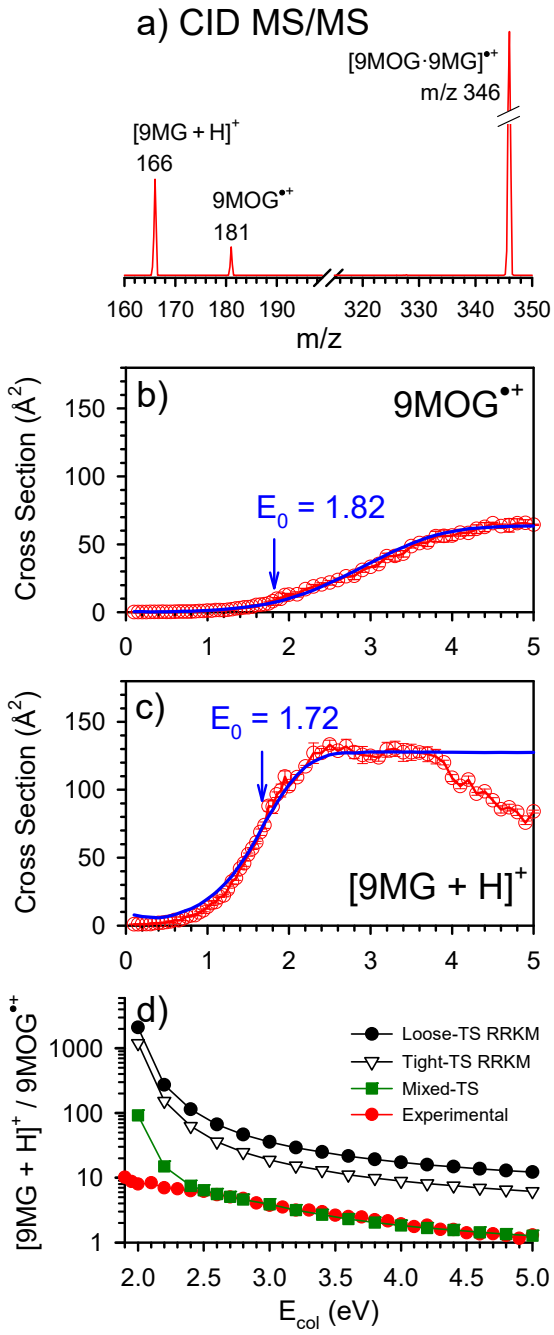
a) CID MS/MS
[9MOG·9MG]•+
m/z 346
[9MG + H]+
166
9MOG•+
181
160 170 180 190 320 330 340 350
m/z
b)
9MOG•+
E0 = 1.82
Cross Section (Å2)
c)
E0 = 1.72
[9MG + H]+
d)
Loose-TS RRKM
Tight-TS RRKM
Mixed-TS
Experimental
[9MG + H]+ / 9MOG•+
Ecol (eV)

Fig. 4

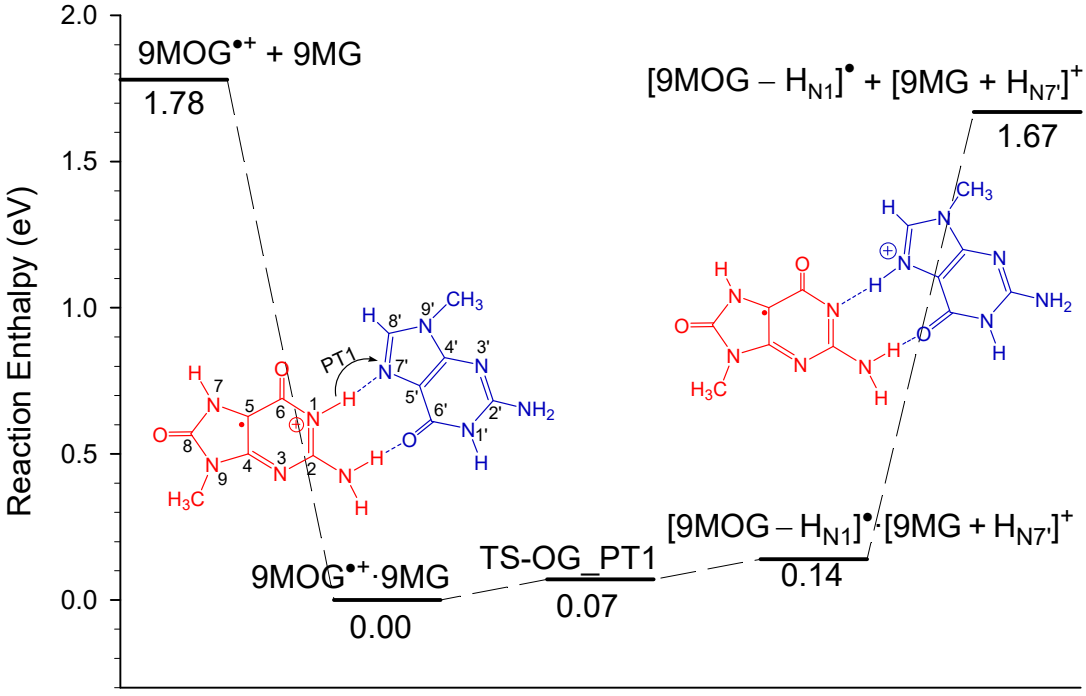
Reaction Enthalpy (eV)
2.0
1.5
1.0
0.5
0.0
9MOG•+ + 9MG
1.78
9MOG•+·9MG
0.00
TS-OG_PT1
0.07
[9MOG – HN1]• + [9MG + HN7']+
1.67
[9MOG – HN1]•·[9MG + HN7']+
0.14
PT1

Fig. 5

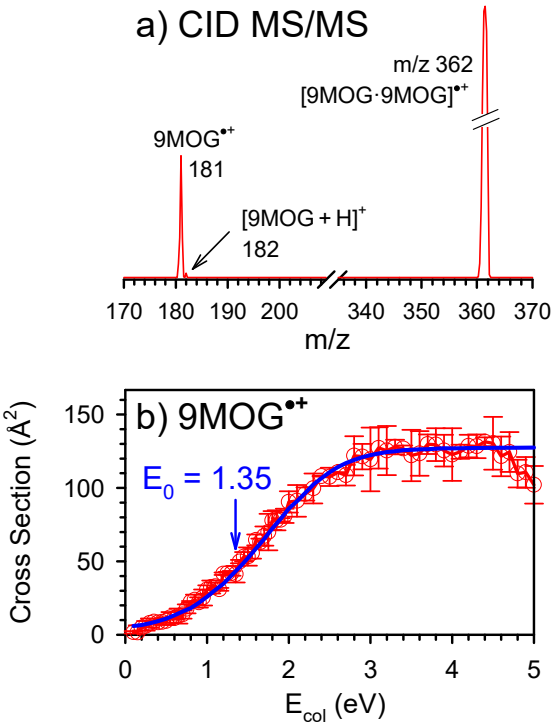
a) CID MS/MS
m/z 362
[9MOG·9MOG]•+
9MOG•+
181
[9MOG + H]+
182
170 180 190 200 340 350 360 370
m/z
b) 9MOG•+
E0 = 1.35
Cross Section (Å2)
150
100
50
0
0 1 2 3 4 5
Ecol (eV)

Fig. 6

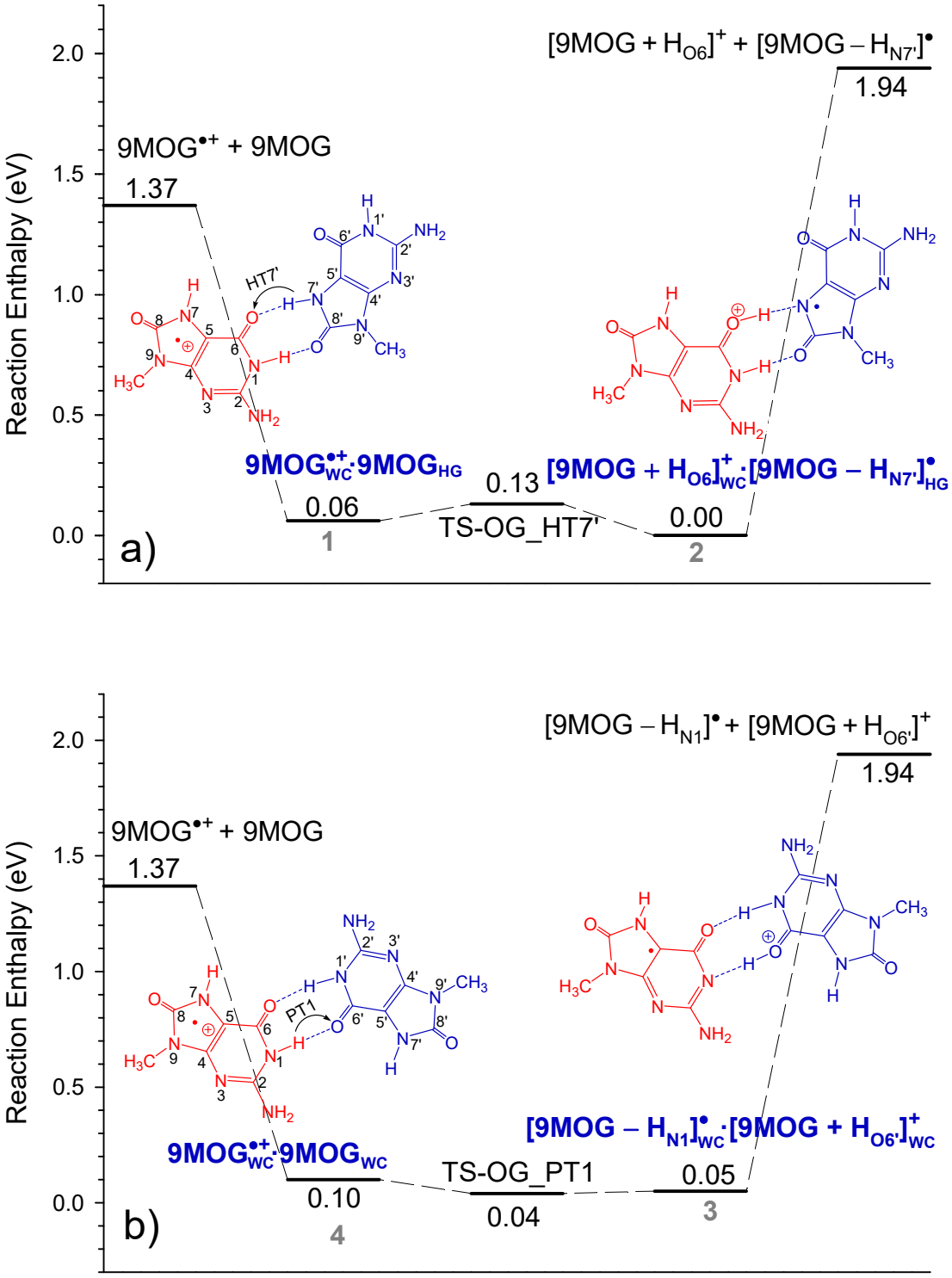
Reaction Enthalpy (eV)
2.0
1.5
1.0
0.5
0.0
9MOG•+ + 9MOG
1.37
[9MOG + H_O6]+ + [9MOG – H_N7']•
1.94
9MOG•+WC·9MOGHG
0.06
1
0.13
TS-OG_HT7'
[9MOG + H_O6]+WC·[9MOG – H_N7']•HG
0.00
2
a)
[9MOG – H_N1]• + [9MOG + H_O6']+
1.94
9MOG•+ + 9MOG
1.37
9MOG•+WC·9MOGWC
0.10
4
TS-OG_PT1
0.04
[9MOG – H_N1]•WC·[9MOG + H_O6']+WC
0.05
3
b)

Graphic for TOC

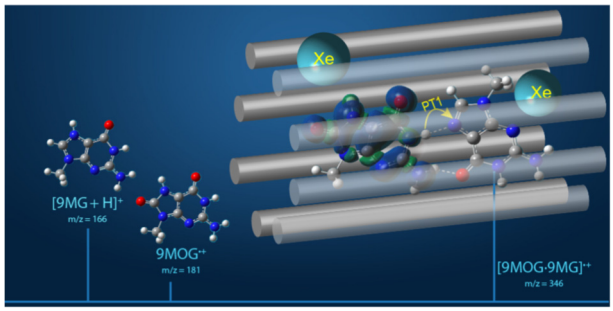

Non-statistical dissociation in heterodimeric 8-oxoguanine–guanine base-pair radical cation